2630 *Inorg. Chem.* **2010**, *49*, 2630–2638
DOI: 10.1021/ic901254j

Inorganic Chemistry
Article

Revisiting the Thermal Decomposition of Layered γ-Titanium Phosphate and Structural Elucidation of Its Intermediate Phases

Santiago García-Granda, Sergei A. Khainakov, Aranzazu Espina, and José R. García

Departamentos de Química Física y Analítica y Química Orgánica e Inorgánica, Universidad de Oviedo, 33006 Oviedo, Spain

Germán R. Castro

SpLine, Spanish CRG Beamline, ESRF, BP 220, F-38043 Grenoble Cedex, France

João Rocha and Luís Mafra*

Department of Chemistry, CICECO, University of Aveiro, 3810-193 Aveiro, Portugal

Received June 30, 2009

The thermal transformations of γ-titanium phosphate, $Ti(PO_4)(H_2PO_4)\cdot 2H_2O$, have been studied by thermal analyses (thermogravimetry (TG) and differential thermal analysis (DTA)) and variable-temperature ^{31}P magic-angle spinning (MAS)/CPMAS and 2D $^{31}P-^{31}P$ spin-exchange NMR. The structure of this material has been refined from synchrotron powder X-ray diffraction data (monoclinic, $P2_1$, $a = 5.1811(2)$ Å, $b = 6.3479(2)$ Å, $c = 23.725(2)$ Å, $\beta = 102.57(1)°$). Vyazovkin's model-free kinetic algorithms have been applied to determine the apparent activation energy to both dehydration and dehydroxylation of γ-titanium phosphate. In these processes, several overlapped steps have been detected. Structural models for $Ti(PO_4)(H_2PO_4)\cdot H_2O$ and $Ti(PO_4)(H_2P_2O_7)_{0.5}$ intermediate layered phases have been proposed.

Introduction

Metal salts of phosphoric acid have been known for over a century. However, research into layered tetravalent metal phosphates and their relatives only began in the late 1950s because of the recognition of the application of some of these salts as cation exchangers in radioactive waste streams.[1] Because of their low solubility, at first, tetravalent metal phosphates were only available as amorphous gels. In 1964, Clearfield and Stynes prepared the first crystalline compound,[2] α-$Zr(HPO_4)_2\cdot H_2O$, which made their layered structure[3,4] and chemical reactivity clearly understood.[5] Since then, the possibility of relating the properties of these metal acid salts to their crystalline structure and the many potential applications in the fields of ion exchange, intercalation, catalysis, and ionic conductivity prompted the comprehensive study of these class of compounds.[6−9]

The existence of the γ-layered compound was also reported by Clearfield et al.,[10] who prepared $Zr(PO_4)(H_2PO_4)\cdot 2H_2O$ and $Zr(PO_4)(H_2PO_4)$. The prefix γ was assigned to the dihydrate and the prefix β to the anhydrous compound. The formula was originally given as γ-$Zr(HPO_4)_2\cdot 2H_2O$. However, ^{31}P MAS NMR studies performed by Clayden[11] showed that γ-ZrP contains tertiary phosphate groups and dihydrogen phosphate groups in equal amounts. In 1990 Christensen et al.[12] proposed a structure for the titanium parent compound, $Ti(PO_4)(H_2PO_4)\cdot 2H_2O$, from powder diffraction data that was in accordance with the results of Clayden. However, the positions of the water molecules were not found, and there was uncertainty concerning the space

*To whom correspondence should be addressed. E-mail: lmafra@ua.pt.

(1) Kraus, K. A.; Phillips, H. O. *J. Am. Chem. Soc.* **1956**, *78*, 644.
(2) Clearfield, A.; Stynes, J. A. *J. Inorg. Nucl. Chem.* **1964**, *26*, 117.
(3) Clearfield, A.; Smith, G. D. *Inorg. Chem.* **1969**, *8*, 431.
(4) Troup, J. M.; Clearfield, A. *Inorg. Chem.* **1977**, *16*, 3311.
(5) Kullberg, L.; Clearfield, A. *J. Phys. Chem.* **1981**, *85*, 1578.
(6) *Inorganic Ion Exchange Materials*; Clearfield, A., Ed.; CRC Press: Boca Raton, FL, 1982.
(7) Alberti, G.; Costantino, U. In *Intercalation Chemistry*; Whitinghan, M. S., Jacobson, A. J., Eds.; Academic Press: New York, 1982.
(8) Alberti, G. In *Recent Developments in Ion Exchange*; Williams, P. A., Hudson, M. J., Eds.; Elsevier Applied Science: London, 1987.
(9) Clearfield, A. In *Design of New Materials*; Plenum Press: New York, 1987.
(10) Clearfield, A.; Blessing, R. H.; Stynes, J. A. *J. Inorg. Nucl. Chem.* **1968**, *30*, 249.
(11) Clayden, N. J. *J. Chem. Soc., Dalton Trans.* **1987**, 1877.
(12) Christensen, A. N.; Andersen, E. K.; Andersen, I. G. K.; Alberti, G.; Nielsen, M.; Lehmann, M. S. *Acta Chem. Scand.* **1990**, *44*, 865.

Published on Web 02/19/2010

Table 1. Unit Cell Dimensions for γ-TiP and Parent Materials

compound	a (Å)	b (Å)	c (Å)	β (deg)	V/Z (Å^3)	ref.
γ-$Ti(PO_4)(H_2PO_4)\cdot 2H_2O$	5.181(1)	6.347(1)	11.881(1)	102.59(1)	190.6	12
γ-$Ti(PO_4)(H_2PO_4)\cdot 2H_2O$	5.186(1)	6.3505(8)	11.865(3)	102.52(3)	190.7	19
γ'-$Ti(PO_4)(H_2PO_4)\cdot(2-x)H_2O$ ($x \sim 1$)	23.670(3)	6.264(1)	5.036(1)	102.41(1)	182.3	18
β-$Ti(PO_4)(H_2PO_4)$	18.9503(4)	6.3127(1)	5.1391(1)	105.366(2)	148.2	14
$Ti(PO_4)(H_2P_2O_7)_{0.5}$	16.271(3)	6.319(1)	5.122(1)	90.59(2)	131.6	18

group. In 1995 the structure of γ-ZrP was solved from powder X-ray diffraction by Poojary et al.,[13] and the data confirmed the model reported by Christensen et al. Later, a structure determination of β-TiP showed that the structure of the γ-type layer is retained in the anhydrous compound.[14]

The γ-TiP dehydration has been described by several authors, and thermal data (derived from thermogravimetry (TG), differential thermogravimetry (DTG), differential thermal analysis (DTA), and differential scanning calorimetry (DSC) curves) have been reported.[15−17] Apparently, the process occurred in two steps, with the formation of an intermediate phase that is difficult to isolate. More recently, Andersen and Norby,[18] based on temperature-resolved in situ powder X-ray diffraction, proposed that the transformation sequence goes from γ-TiP over a partially dehydrated form, γ'-$Ti(PO_4)(H_2PO_4)\cdot(2-x)H_2O$ ($x \sim 1$), denoted as γ'-TiP, to the anhydrous form β-TiP. According to these authors, the new γ'-TiP phase has a monoclinic unit cell related to γ-TiP (see Table 1).

When the β-TiP is heated, hydroxyl condensation takes place. Costantino and La Ginestra[20] propose that this process leads to the formation of a layered pyrophosphate. They suggest that the hydroxyl condensation initially leads to the formation of a pyrophosphate phase with a structure similar to that of the starting material, but with adjacent layers joined by P−O−P bridges. Later, Andersen and Norby,[18] concluded that the first part of the hydroxyl condensation occurs without or with only slight alterations in the layer structure, but with a variable basal spacing caused by partial hydroxyl condensation. Although the temperature range of pure layered pyrophosphate is very narrow, they propose the formation of one P−O−P bridge per dihydrogen phosphate group, which gives a compound with the formula $Ti(PO_4)(H_2P_2O_7)_{0.5}$ (see Table 1).

In previous contributions, we have described the behavior of the γ-titanium phosphate as ion-exchanger,[21−23] its very high affinity to cesium ions,[24] and the synthesis of three-dimensional compounds by heating the alkali-metal ion-exchanged phases.[25] Here, we revise the structural and thermal data of the family head compound, γ-titanium phosphate, using a combination of scientific methods that had never been applied jointly to explore and clarify the thermal decomposition behavior of this material.

Experimental Section

Sample Preparation and Analytical Procedures. The synthesis of γ-TiP was performed as previously reported.[17] Phosphorus and titanium contents were determined by inductively coupled plasma mass spectrometry (ICP-MS) analysis (Finnigan, Element model) after dissolving 0.5 g of the sample in HF(aq). A Mettler-Toledo TGA/SDTA851^e is used for the thermal analyses in nitrogen dynamic atmosphere (50 mL/min) at a heating rate of 10 °C/min. Four individual samples were obtained by thermal treatment of γ-TiP (150 ± 1 mg each), also at a heating rate of 10 °C/min, from room temperature until 300 °C, 500 °C, 700 °C, or 900 °C; when the preset temperature is reached, the samples were immediately taken out of the muffle and cooled in the laboratory ambient. The experimental weight loss percentage in the heating processes was 13.0, 16.7, 18.5, and 20.1, respectively (calculated for the formation of $Ti(PO_4)(H_2PO_4)$, $Ti(PO_4)(H_2P_2O_7)_{0.5}$, and TiP_2O_7: 13.05, 16.30, and 19.57, respectively).

NMR Studies. ^{31}P SPE (single-pulse experiment) MAS and CPMAS NMR spectra were recorded at 161.9 MHz on a Bruker Avance 400 (9.4 T) wide-bore spectrometer (DSX model) using a 4 mm CPMAS probe. An excitation pulse length of 2 μs (45° flip-angle), recycle delay of 100 s, ^{1}H heteronuclear decoupling (TPPM) strength of 100 kHz and MAS rate of 12 kHz were employed for all the experiments. In addition, a very short contact time (CT = 50 μs) was used for ^{31}P CPMAS NMR experiments. ^{31}P SPE MAS NMR spectra were recorded at temperatures ranging from room temperature to 120 °C using a Bruker BVT 3000 unit. At each temperature, an interval of 30−60 min was employed prior to recording the ^{31}P NMR spectra. 2D ^{31}P−^{31}P spin-exchange NMR spectrum was recorded using 90° excitation pulse lengths of 3.6 μs, mixing times between 0.1 and 2 s, recycle delay of 20 s (a saturation comb of ^{31}P pulses were used at the beginning of the experiments). The States−Haberkorn−Ruben (SHR) acquisition method was used to obtain phase sensitive detection during t_1 evolution. Additional NMR details are depicted on the figure captions. ^{31}P chemical shifts are depicted in parts per million (ppm) with respect to 85% H_3PO_4.

Diffraction Studies. Powder X-ray diffraction patterns were collected on an X'Pert PRO MPD X-ray diffractometer with PIXcel detector, operating in the Bragg−Brentano ($\theta/2\theta$) geometry, CuK_α radiation (λ = 1.5418 Å). The γ-TiP powder synchrotron X-ray diffraction pattern was recorded on beamline BM25A (Spanish CRG, SpLine) at the European Synchrotron Radiation Facility (ESRF), Grenoble (France). The sample was finely ground and loaded into a 1.0 mm diameter capillary mounted in a spinning goniometer. Room-temperature data were collected in a continuous 2θ-scan mode from 2.4° to 60° using an incident wavelength of 0.82626(6) Å (calibrated with

(13) Poojary, D. M.; Shpeizer, B.; Clearfield, A. *J. Chem. Soc., Dalton Trans.* **1995**, 111.
(14) Andersen, A. M. K.; Norby, P.; Vogt, T. *J. Solid State Chem.* **1998**, *140*, 266.
(15) La Ginestra, A.; Massucci, M. A. *Thermochim. Acta* **1979**, *32*, 241.
(16) Kobayashi, E.; Yamazaki, S. *Bull. Chem. Soc. Jpn.* **1983**, *56*, 1632.
(17) Llavona, R.; García, J. R.; Suárez, M.; Rodríguez, J. *Thermochim. Acta* **1985**, *86*, 281.
(18) Andersen, A. M. K.; Norby, P. *Inorg. Chem.* **1998**, *37*, 4313.
(19) Salvadó, M. A.; García-Granda, S.; Rodríguez, J. *Mater. Sci. Forum* **1994**, *166−169*, 619.
(20) Costantino, U.; La Ginestra, A. *Thermochim. Acta* **1982**, *58*, 179.
(21) Álvarez, C.; Llavona, R.; García, J. R.; Suárez, M.; Rodríguez, J. *Inorg. Chem.* **1987**, *26*, 1045.
(22) Álvarez, C.; Llavona, R.; García, J. R.; Suárez, M.; Rodríguez, J. *J. Chem. Soc., Dalton Trans.* **1987**, 2045.
(23) Llavona, R.; Suárez, M.; García, J. R.; Rodríguez, J. *Inorg. Chem.* **1989**, *28*, 2863.
(24) González, E.; Llavona, R.; García, J. R.; Rodríguez, J. *J. Chem. Soc., Dalton Trans.* **1989**, 1825.
(25) Salvadó, M. A.; Pertierra, P.; García-Granda, S.; Suárez, M.; Rodríguez, M. L.; Llavona, R.; García, J. R.; Rodríguez, J. *J. Mater. Chem.* **1996**, *6*, 415.

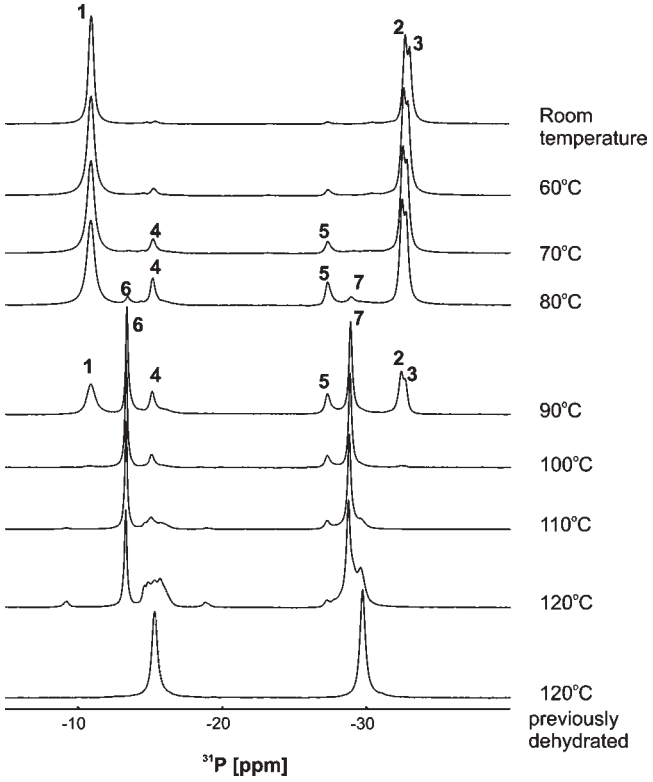

Figure 1. ^{31}P SPE MAS NMR spectra of γ-TiP recorded at the temperatures indicated. Labels are added to at least three different phases to facilitate the tracking of different phase changes with temperature variation. Peak labels: 1, 2, and 3 for γ-TiP phase; 4, 5 for anhydrous environments in the γ- and/or γ'-TiP interlayer space; 6 and 7 for the γ'-TiP phase.

NIST SRM 640c silicon powder; a = 5.431195(9) Å).[26] The counts from the different channels were rebinned to produce an equivalent normalized step scan of 0.02° step intervals, with a count time of 5 s per step. Indexing was performed with TREOR90 and ITO12 which are included in the CRYSFIRE suite.[27] A monoclinic cell with a = 5.181 Å, b = 6.351 Å, c = 11.878 Å, and β = 102.672°, F_{20} = 31 (0.012449, 52) (by TREOR) and an orthorhombic cell with a = 6.3437 Å, b = 23.1496 Å, c = 5.1788 Å (by ITO) were found. Cell parameters are similar to the previously reported.[12,19] In the previous structural models (both orthorhombic and monoclinic) the unit cell contains only two independent crystallographic phosphorus, in contrast with ^{31}P SPE MAS NMR that shows the existence of four crystallographically distinct P sites (Figure 1, top). Two P sites resonate at about −32.5 ppm (labels 2 and 3 from Figure 1) while two other superimposed P sites resonate at about −11 ppm (label 1 from Figure 1). For this reason, Rietveld refinement of the pattern using the partial structural model based on the Christensen proposal, with duplicated c-axis, was carried out in the program GSAS.[28] Initial least-squares refinements of the profile included terms for the scale factor, background, lattice parameters, zero point, and peak shape. A series of difference Fourier maps, computed at this stage, revealed peaks corresponding to the approximate positions of the remaining atoms in the structure. Atomic positions were refined with soft constraints consisting of Ti−O, P−O, and O−O bond distances. During the final cycles of refinement, the weight for the soft constraints was reduced but could not be completely released for O5, O7 and Ow1, Ow3. The refinement of the positional parameters, as well as their thermal parameters at this stage, converged with R_{wp} = 0.125. The crystallographic data are given in Table 2, and the final Rietveld difference plot is given in Figure 2.

Table 2. Crystal Data of γ-TiP

formula	$Ti(PO_4)(H_2PO_4)\cdot 2H_2O$
formula weight	275.86
crystal system	monoclinic
space group	$P2_1$ (No. 4)
a/Å	5.1811(2)
b/Å	6.3479(2)
c/Å	23.725(2)
β/deg	102.57(1)
Z	4
R_p	0.0946
R_{wp}	0.1252
R_F^2	0.1455
χ^2	1.7

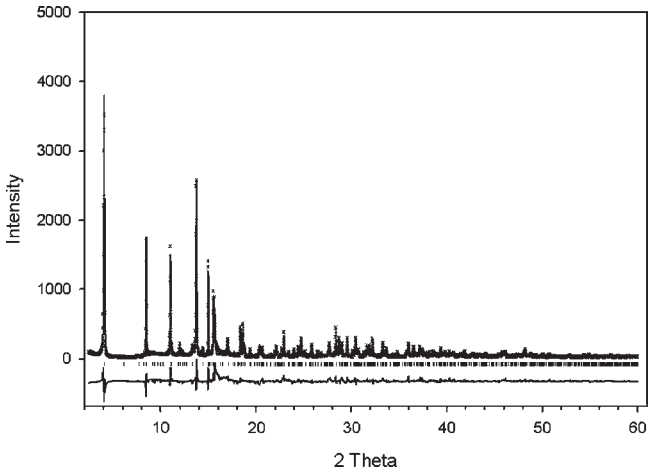

Figure 2. Powder synchrotron X-ray diffraction pattern of γ-TiP. Observed (×), calculated (continuous line), background (line), and difference (below) profiles are plotted on the same scale.

Structural Modeling. For the phases listed in Table 1, only γ'-$Ti(PO_4)(H_2PO_4)\cdot(2-x)H_2O$ ($x \sim 1$) and $Ti(PO_4)(H_2P_2O_7)_{0.5}$ structures are not reported. The γ'-TiP cell parameters (see Table 1) are related to the ones reported here for γ-TiP (see Table 2). As a consequence, in a first step, the γ-titanium phosphate sheets were displaced until reaching the interlayer distance of γ'-TiP, and the initial atomic coordinates for the P, Ti, and O atoms were estimated with the ATOMS program.[29] After removing half of the water molecules, the γ-$Ti(PO_4)(H_2PO_4)\cdot H_2O$ geometry was optimized with the FORCITE module in the Materials Studio modeling environment. FORCITE is a computational module, which estimates the total sublimation energy and packing of molecular crystals. An all-purpose universal force field was used in the optimization. The charges in the system are calculated using the QEq-method (charge equilibrium approach). The asymmetric unit of the crystal structure was divided into fragment-based rigid units. After several geometry optimization runs, the conformation with smaller relative energy was selected. In the same way, the $Ti(PO_4)(H_2P_2O_7)_{0.5}$ structure model was obtained starting from the β-$Ti(PO_4)(H_2PO_4)$ crystal data. Now, the β-titanium phosphate sheets were displaced until reaching the interlayer distance of $Ti(PO_4)(H_2P_2O_7)_{0.5}$ pseudolayered compound (see Table 1), and the initial atomic coordinates for the P, Ti, and O atoms were estimated by ATOMS.[38] After removing a fourth part of the interlayer oxygen atoms (POH groups), the system geometry

(26) National Institute of Standards and Technology, Department of Commerce, U.S.A. http://www.nist.gov/srm. (accessed Nov **2007**).

(27) Shirley, R. *The CRYSFIRE System for Automatic Powder Indexing: User's Manual*; Lattice Press: Guildford, Surrey, U.K., 2000.

(28) Larson, A.; Von Dreele, R. B. *GSAS: Generalized Structure Analysis System*; Los Alamos National Laboratory: Los Alamos, NM, 1994.

(29) www.shapesoftware.com.

was optimized with FORCITE. Convergence criteria for two compounds are chosen according to the FORCITE ultrafine settings, which corresponds to a convergence of the energies of better than 2×10^{-5} kcal/mol and of the residual forces of better than 1×10^{-3} kcal/(mol Å), and we obtained the following output (root-mean-square (rms) force and max force, in kcal/(mol Å), respectively): γ-$Ti(PO_4)(H_2PO_4)\cdot H_2O$ (2.000×10^{-4} and 3.951×10^{-4}) and $Ti(PO_4)(H_2P_2O_7)_{0.5}$ (1.575×10^{-4} and 6.152×10^{-4}). In the final models, the hydrogen atoms were geometrically located with MERCURY.[30]

Determination of Kinetic Parameters. The rate of heterogeneous solid-state reactions can be generally described by:

$$\frac{d\alpha}{dt} = k(T) f(\alpha) \quad (1)$$

where t is the time, $k(T)$ is the temperature-dependent constant, and $f(\alpha)$ is a function called the reaction model, which described the dependence of the reaction rate on the extent of reaction, α. The temperature dependence of the rate constant is described by the Arrhenius equation. Then, the rate of a solid-state reaction can be generally described by:

$$\frac{d\alpha}{dt} = A e^{-E/RT} f(\alpha) \quad (2)$$

where A is the pre-exponential factor, E, the activation energy, and R, the gas constant. The above rate expression can be transformed into non-isothermal rate expressions describing reaction rates as a function of temperature at a constant heating rate, β.

$$\frac{d\alpha}{dT} = \frac{A}{\beta} e^{-E/RT} f(\alpha) \quad (3)$$

Model-free isoconversion methods allow estimating the activation energy as a function α without choosing the reaction model. The basic supposition of these methods is that the reaction rate for a constant extent of conversion, α, depends only on the temperature.[31−33] Hence, constant E values can be expected in the case of single state decomposition while a multistep process E varies with α due the variation in the relative contributions of single step to the overall reaction rate. In non-isothermal kinetics, several isoconversional methods were proposed. To use these methods, a series of experiments has to be conducted at different heating rates.[34,35] Vyazovkin et al. developed an isoconversional method which allows evaluating both simple and complex reactions.[36] Integrating up to conversion, α, eq 3, gives

$$\int_0^\alpha \frac{d\alpha}{f(\alpha)} = g(\alpha) = \frac{A}{\beta} \int_{T_0}^{T} e^{-E/RT}\, dT \quad (4)$$

Since $E/2RT \gg 1$, the temperature integral can be approximated by

$$\int_{T_0}^{T} e^{-E/RT}\, dT \approx \frac{R}{E} T^2 e^{-E/RT} \quad (5)$$

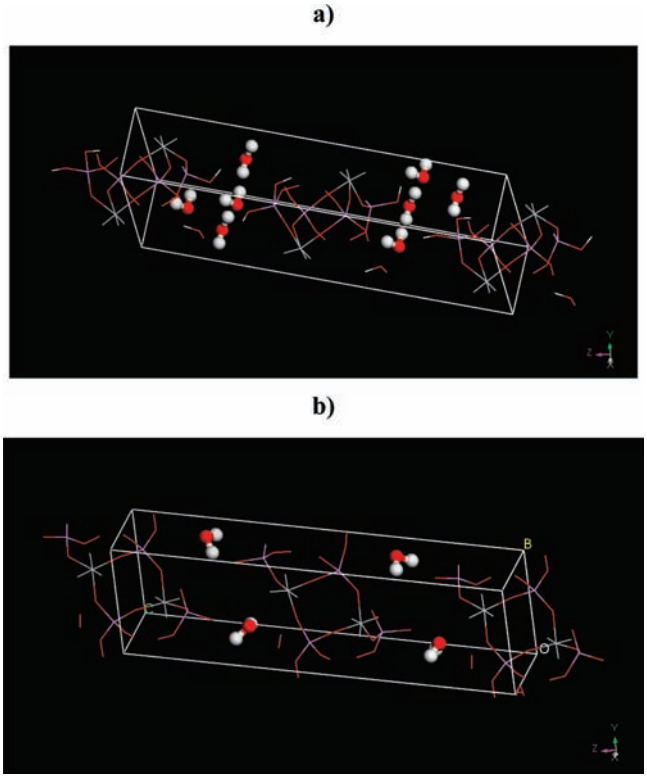

Figure 3. Crystal packing of layered titanium phosphates represented by mixed ball-and-stick (guest molecules) and stick (inorganic sheet) representations, viewed along the *a*-axis: (**a**) γ-TiP, and (**b**) γ'-TiP.

Substituting the temperature integral and taking the logarithm gives

$$\ln \frac{\beta}{T_\alpha^2} = \ln \left[\frac{RA}{E_\alpha g(\alpha)}\right] - \frac{E_\alpha}{R} \frac{1}{T_\alpha} \quad (6)$$

To apply the method, it is necessary to obtain the experimental data at least at three different heating rates (β), and the respective conversion curves are evaluated from the measured TG curves.[35] For each conversion (α), $\ln(\beta/T_\alpha^2)$ plotted versus $1/T_\alpha$ gives a straight line with slope $-E_\alpha/R$; therefore, the activation energy is obtained as function of the conversion.

Results and Discussion

^{31}P NMR and powder synchrotron X-ray diffraction data show that although the γ-$Ti(PO_4)(H_2PO_4)\cdot 2H_2O$ layer is similar to that found by Christensen et al., in the latter the unit cell was inadequately selected (see Tables 1 and 2). The structure is built from TiO_6 octahedra and phosphate tetrahedral (PO_4 and $(OH)_2PO_2$). All four oxygen atoms of the tertiary phosphate group bind to titanium. In the dihydrogen phosphate group two oxygen atoms bind to titanium while the other two oxygen atoms point toward the interlamellar space (where water molecules are present) as hydroxyl groups (Figure 3a).

In spite of the tendency to simplify the chemical reaction mechanisms, reality is often complex.[36] In particular, in layered tetravalent metal phosphates, the processes that include composition changes in the interlayer space rarely lapse with the coexistence of only two defined crystalline phases, which contradicts several previous proposals.[37,38]

(30) http://www.ccdc.cam.ac.uk/mercury/
(31) Maichrzak-Kuceba, I.; Nowak, W. *Thermochim. Acta* **2004**, *413*, 23.
(32) Polli, H.; Pontes, L. A. M.; Araujo, A. S. *J. Therm. Anal. Calorim.* **2005**, *79*, 383.
(33) Vecchio, S.; Rocco, R. D.; Ferragina, C.; Materazzi, S. *Thermochim. Acta* **2005**, *435*, 181.
(34) Vyazovkin, S. *Int. Rev. Phys. Chem.* **1998**, *17*, 407.
(35) Vyazovkin, S.; Wight, C. A. *Thermochim. Acta* **1999**, *53*, 340.
(36) Costantino, U.; Vivani, R.; Zima, V.; Cernoskova, E. *J. Solid State Chem.* **1997**, *132*, 17.
(37) García, J. R.; Suárez, M.; Rodríguez, J. *Anal. Chem.* **1984**, *56*, 193.
(38) Llavona, R.; Suárez, M.; García, J. R.; Rodríguez, J. *Anal. Chem.* **1986**, *58*, 547.

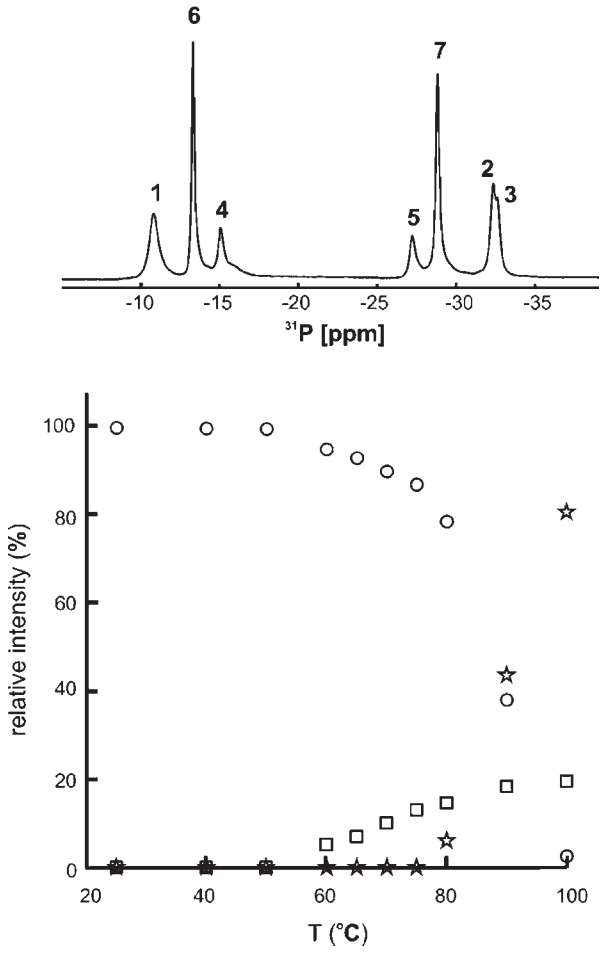

Figure 4. Relative intensities (areas) of the ^{31}P NMR resonances (indicated in the top spectrum), given by three main TiP phases, as a function of temperature (spectra in Figure 1); peak labeling: 1, 2, 3 (○); 4, 5 (□); 6, 7 (☆). Asterisks depict non-protonated (PO_4/P_2O_7) phosphorus groups.

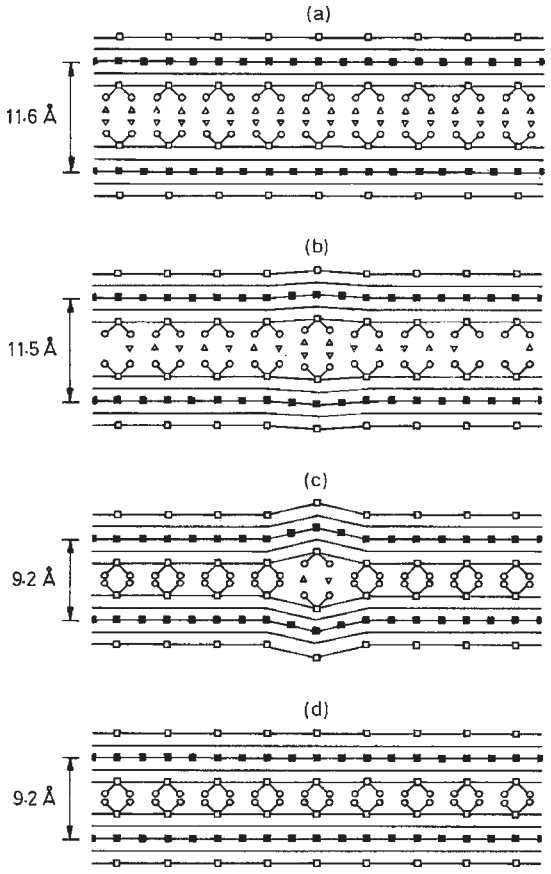

Figure 5. Proposed γ-TiP transformations from a dihydrated phase (**a**) to β-TiP anhydrous phase (**d**): partial dehydration takes place almost without basal spacing change, and di-, mono-, or/and unhydrated environments coexist in the interlayer space (**b**) prior to the formation of the anhydrous phase with a drastic reduction to the basal spacing (**c**). ○ indicates OH groups; ▽ and △ indicate H_2O molecules.

For the thermal decomposition of γ-TiP, the transformation sequence (accepted at present) implies the formation of a partially dehydrated form γ'-Ti(PO_4)(H_2PO_4)·$(2 - x)H_2O$ ($x \sim 1$) prior to the formation of the anhydrous form (β-TiP).[18] However, the ^{31}P SPE MAS NMR data (see Figure 1) indicate that the process is more complex. Using the same peak labels as indicated in Figure 4, we observe that as the temperature increases until 100 °C, the γ-TiP ^{31}P signals (1−3) become less intense until they disappear at 100−110 °C. Simultaneously, two faint ^{31}P resonances appear (4 and 5) and, later, they coexist with another pair of signals (6 and 7) whose intensity increases suddenly between 80 and 90 °C accompanied by a considerable intensity decrease of the γ-TiP ^{31}P signals (1, 2, and 3). Above 100 °C, γ-TiP ^{31}P signals (1−3) vanish, and several ^{31}P resonances are observed in the typical chemical shift region of the anhydrous material (Figure 1, bottom). The ^{31}P resonances 6 and 7 (1:1 ratio) are, thus, assigned to the γ'-TiP phase.

Previously, to obtain information about the structural changes that take place during the formation of γ'-TiP, the temperature dependence of the unit cell volume and the lattice parameters were investigated.[18] Powder X-ray diffraction (XRD) data indicates that the decrease in unit cell volume, when γ'-TiP is formed, is not due to the slight decrease in interlayer distance (from 11.588 to 11.565 Å). Instead, it is caused by a shortening of the b and c axes (by 1.2 and 2.8%, respectively), not by a decrease in the interlayer parameter (a sin β)/2. Hence, the ^{31}P NMR signals that remain unassigned (peaks 4 and 5, Figure 4) are ascribed to anhydrous environments in the γ- and/or γ'-TiP interlayer space (Figure 5a,b). At this stage, it is worth mentioning that the 1:1 ^{31}P peak integration ratio extracted from 1D spectra and the 2D ^{31}P−^{31}P spin-exchange NMR experiment (Figure 6) show that, for example, resonances 4 and 5 belong to the same phase. The ^{31}P−^{31}P spin-exchange spectrum, clearly shows the existence of a single cross-peak between 4 and 5 (anhydrous environments in the γ- and/or γ'-TiP phases) and between 1 and 2,3 (γ-TiP phase) peaks thus confirming that 4 and 5 P sites are close in space (i.e., they are part of the same phase) as well as 1 and 2,3 P sites (Figure 6).

The TG curve of γ-TiP (very similar to that reported in ref 18) is shown in Figure 7. Several of the observed steps (B, C, E, and F) have been previously explained:

$$\gamma\text{-Ti}(PO_4)(H_2PO_4)\cdot 2H_2O \rightarrow \gamma'\text{-Ti}(PO_4)(H_2PO_4)\cdot (2-x)H_2O \rightarrow \beta\text{-Ti}(PO_4)(H_2PO_4) \rightarrow \text{Ti}(PO_4)(H_2P_2O_7)_{0.5} \rightarrow TiP_2O_7 \quad (7)$$

However, other well-differentiated stages (D and G), also previously described, and an overlapped process, observed in

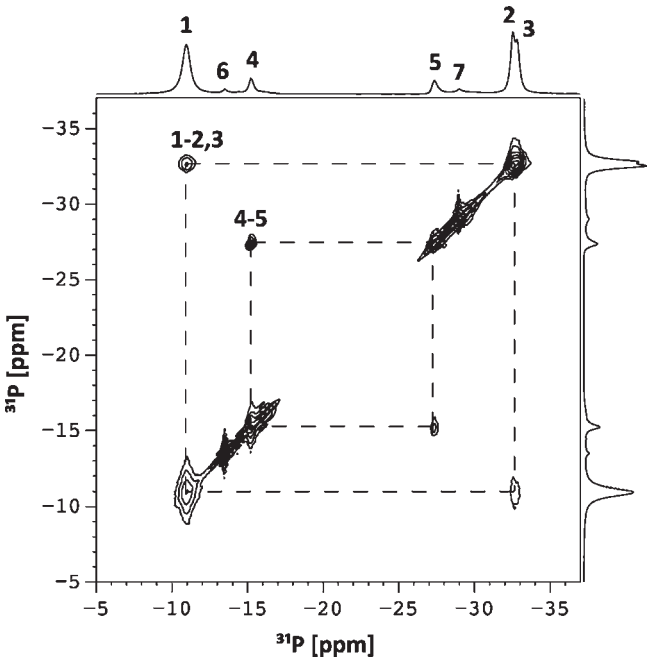

Figure 6. 2D ^{31}P−^{31}P- spin-exchange spectrum of γ-TiP recorded at 80 °C employing a mixing time of 800 ms. The dashed lines depict the off-diagonal cross-peaks connecting ^{31}P resonances from the same phase.

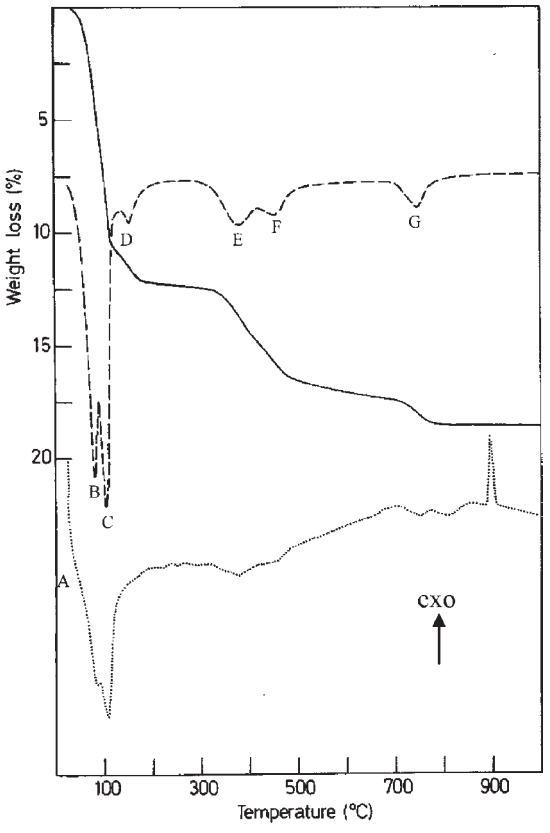

Figure 7. TG (solid line), DTG (dashed line), and DTA (dotted line) curves of γ-TiP (heating rate of 10 °C/min).

this work as a small shoulder in the SDTA-curve (A), remain to be assigned.

Figure 8 shows the TG curves for the thermal decomposition of γ-TiP at three different heating rates. It is observed that although the heating rate does not affect the mass loss, it

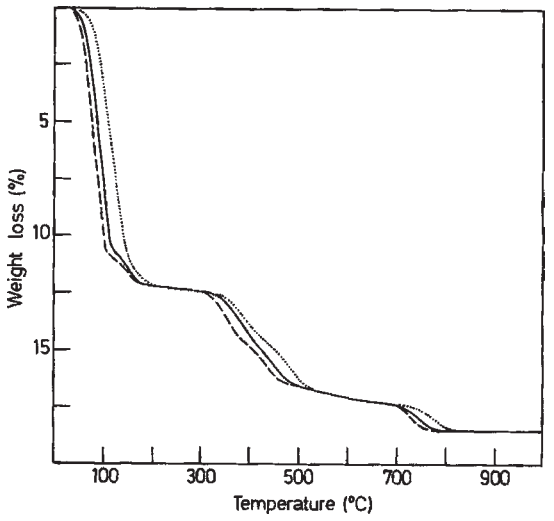

Figure 8. γ-TiP TG curves as a function of heating rate (°C/min): 5 (dashed line), 10 (solid line), and 20 (dotted line).

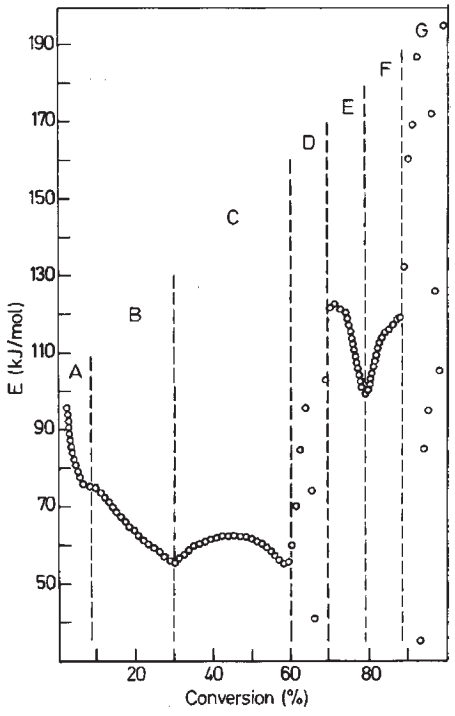

Figure 9. Dependence of the activation energy on the extent of conversion in the γ-TiP thermal decomposition (A−G code as Figure 6).

has an effect on the shape of the TG curve that goes to higher temperatures as the heating rate increases. Application of the Vyazovkin's model free method from these curves allows us to calculate the variation of the activation energy with the conversion of the decomposition reaction (Figure 9).

The dehydration takes place for moderate temperatures ($T < 250$ °C). In Figure 9, the region A (conversion $< 8\%$), where the activation energy decreases with an increase in the conversion, should be related with the existence of a solid solution, γ-Ti$(PO_4)(H_2PO_4)\cdot(2H_2O)_z$ ($z = 0.88-1.00$), with a variable occupancy factor (decreases when increasing the temperature) for the water positions in the γ-TiP structure. For all solid solution compositions, very similar powder XRD patterns should be obtained (see Figure 10). However,

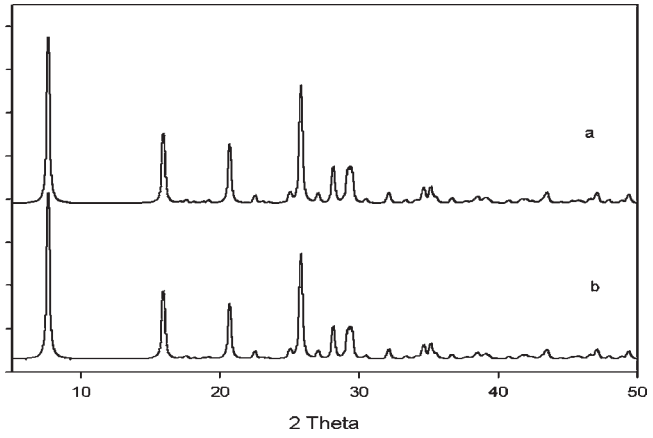

Figure 10. Simulated powder XRD patterns for γ-Ti$(PO_4)(H_2PO_4)\cdot(2H_2O)_z$: (**a**) $z = 1.0$, and (**b**) $z = 0.9$.

the decrease in the hydration degree may be detected by peak integration of the ^{31}P NMR data. The integration of the ^{31}P NMR spectrum obtained at 75 °C, just prior to formation of γ'-TiP phase (labels 6 and 7, Figure 1), indicates that the amount of phosphorus with hydrated environments is about 87% (Figure 4, bottom). At higher conversion degrees (Figure 9, region B) the formation of γ'-Ti$(PO_4)(H_2PO_4)\cdot(2-x)H_2O$ ($x \sim 1$) from γ-Ti$(PO_4)(H_2PO_4)\cdot(2H_2O)_z$ ($z < 1$) takes place (Figure 2b shows the structural model proposed for γ'-TiP).[39] In region C, the nucleation of β-TiP (probably located on the crystal surface) causes a drastic reduction in the interlayer distance, leading to a reduction on the capacity of water diffusion, thus, changing the reaction mechanism and, in a concomitant way, the activation energy trend. Finally, at $T > 130$ °C the dehydration is completed (D band, Figure 7). For this last dehydration step, the calculated activation energy shows random values (Figure 9, region D), which may be interpreted as a consequence of both violent and erratic vaporization of the small water quantities occluded inside the material, whose external basal spacing has already collapsed (Figure 5c). The ^{31}P SPE MAS NMR spectrum recorded at 120 °C (maximum temperature handled by our NMR probe) shows that near such temperature an ensemble of slightly different POH ^{31}P chemical environments (Figure 1, about −14 to −17 ppm), appearing in the dehydrated ^{31}P chemical shift region, coexists. Thus, such diversity of POH groups, corresponding to the anhydrous phase (β-TiP), further supports the existence of multiple layer defects such as the one illustrated in Figure 5, caused by adjacent hydrated POH environments, arranged arbitrarily inside the layer.

At higher temperatures ($T > 300$ °C) dehydroxylation takes place in three differentiated steps. In the first step, when the activation energy decreases with the conversion (Figure 9, region E), the formation of layered Ti$(PO_4)(H_2P_2O_7)_{0.5}$ on the surface of the crystals is expected (Figure 11a,b). Later, two simultaneous processes may occur (Figure 9, region F): formation of Ti$(PO_4)(H_2P_2O_7)_{0.5}$ in the bulk material (product of thermodynamic control) and collapse of the two-dimensional structure on the crystal surface with formation of three-dimensional TiP_2O_7 (product of kinetic control) where the competition between the kinetic and thermodynamic factors (Figure 11c) determines the nature of the material (Figure 12 shows the structural model proposed for Ti$(PO_4)(H_2P_2O_7)_{0.5}$). Finally, as previously described for the dehydration process, the dehydroxylation ends in a sequence of chaotic processes because of the expulsion of the water molecules formed in the most inaccessible sites (product of the condensation reaction of the last hydrogenphosphate groups) with formation of TiP_2O_7 (Figure 7, region G).

To validate the hypothesis proposed for the thermal dehydroxilation process, we have carried out both powder XRD and ^{31}P SPE MAS/CPMAS NMR experiments after

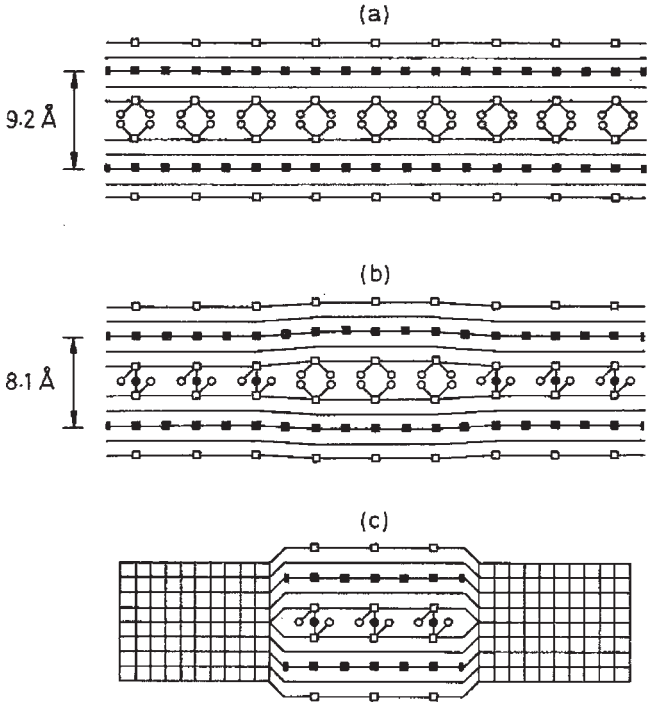

Figure 11. Proposed β-TiP transformation from the layered anhydrous phase (**a**) to titanium pyrophosphate: partial dehydroxylation takes place with basal spacing decreasing, and two environments, Ti$(PO_4)(H_2PO_4)$ and Ti$(PO_4)(H_2P_2O_7)_{0.5}$, coexist in the same sheet (**b**) previously to the formation of three-dimensional TiP_2O_7 in the external part of the crystals (**c**). ○ indicates OH groups; ● indicates oxygen atoms; square mesh indicates the layered habit loss.

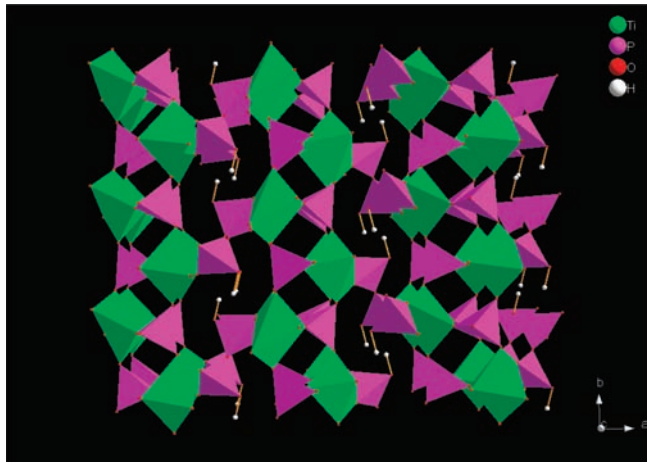

Figure 12. Model crystal packing for Ti$(PO_4)(H_2P_2O_7)_{0.5}$ represented by a mixed ball-and-stick (interlayer connection) and polyhedral (inorganic sheet) representation, viewed along the *c*-axis.

(39) Alberti, G.; Grassi, A.; Lombardo, G. M.; Pappalardo, G. C.; Vivan, R. *Inorg. Chem.* **1999**, *38*, 4249.

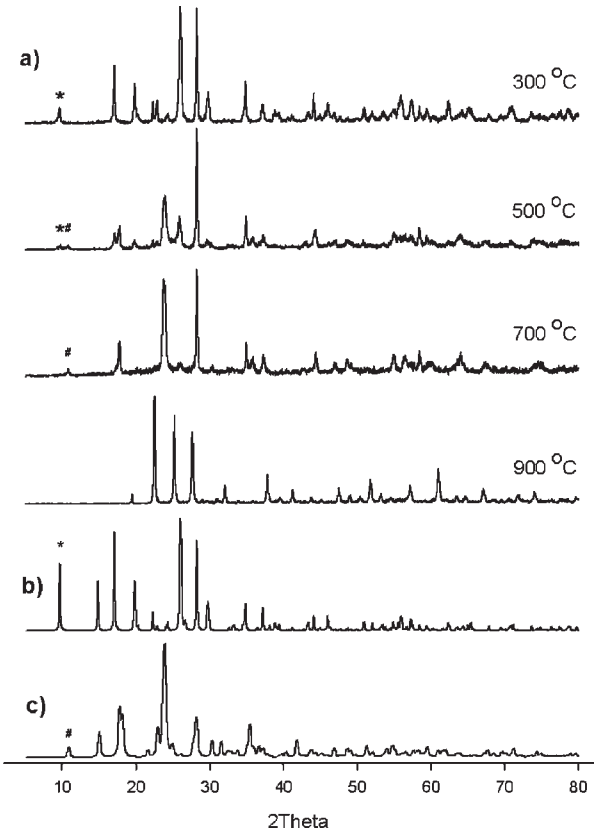

Figure 13. Powder XRD patterns of γ-TiP recorded at room temperature after thermal treatment at temperatures between 300 and 900 °C (**a**), and simulated pXRD patterns for β-$Ti(PO_4)(H_2PO_4)$ (**b**) and $Ti(PO_4)(H_2P_2O_7)_{0.5}$ (**c**). The angular position of the 002 reflections corresponding to β-$Ti(PO_4)(H_2PO_4)$ and $Ti(PO_4)(H_2P_2O_7)_{0.5}$ phases are indicated by * and #, respectively.

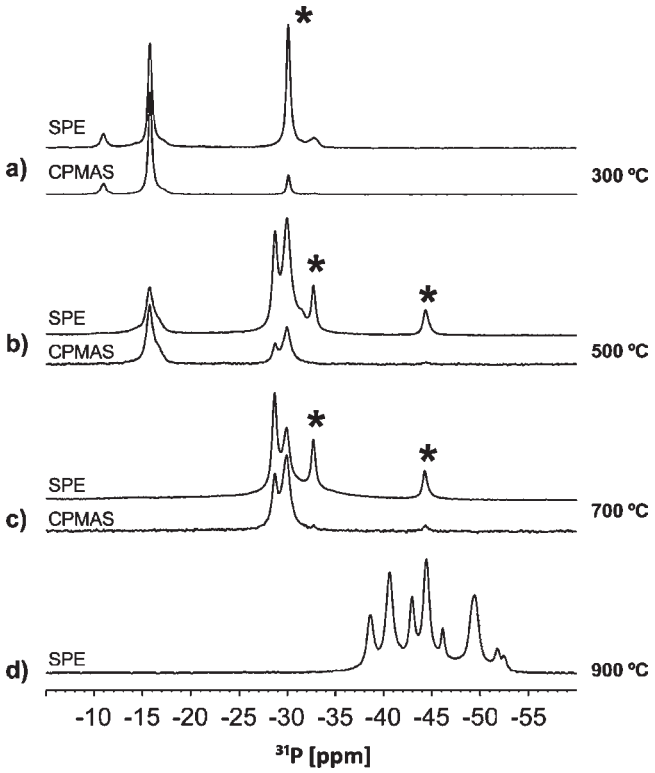

Figure 14. ^{31}P SPE MAS (a−d) and CPMAS (a−c) NMR spectra of γ-TiP recorded at room temperature after thermal treatment at $300 \leq T \leq 900$ °C.

sample treatment at temperatures between 300 and 900 °C (see Experimental Section for details) as shown in Figures 13 and 14. In accordance with previous studies,[18] apparently, diffraction data are easily interpretable. The XRD pattern of the sample obtained at 300 °C essentially coincides with the one reported for β-$Ti(PO_4)(H_2PO_4)$ (cf. Figures 13a and 13b), where the solid treated at 700 °C should be associated to the $Ti(PO_4)(H_2P_2O_7)_{0.5}$ phase (cf. Figures 13a and 13c). At intermediate temperatures (see XRD pattern at 500 °C) a mixture of both phases is detected, and, finally, at 900 °C, cubic TiP_2O_7 phase is obtained (Figure 13a). However, NMR data gives additional insight in phase identification and shows that the thermal decomposition is a more complex process. At 300 °C, the two main ^{31}P resonances present in Figure 14a, at about −16 and −30 ppm, are exactly coincident with the two resonances observed after thermal treatment at 120 °C of the previously dehydrated γ-TiP phase (Figure 1, bottom), that is, β-$Ti(PO_4)(H_2PO_4)$, where the two faint resonances should be assigned to a residue of γ-TiP, practically invisible to X-rays. At 500 °C the ^{31}P NMR spectra changes significantly evidencing the presence of additional phases (Figure 14b). The β-$Ti(PO_4)(H_2PO_4)$ (with resonances at ca. −16 and −30 ppm) now coexist with at least two additional phases with resonances at about −29, −30, −33, and −44 ppm. At higher temperature, β-$Ti(PO_4)(H_2PO_4)$ is being gradually replaced by the new phases, and is completely converted at 700 °C (Figure 14c). The ^{31}P CPMAS experiments carried out at different thermal treatments (Figure 14a−c) have been recorded to help in assigning the protonated phosphorus environments because this technique is sensitive to $^1H-^{31}P$ nuclear spatial proximities, and only ^{31}P resonances in protonated environments are essentially polarized. Comparing ^{31}P NMR spectra obtained with both SPE MAS and CPMAS techniques, the latter filters-out non-protonated phosphorus environments, and thus it is possible to discriminate between protonated (H_2PO_4/$H_2P_2O_7$) and non-protonated (PO_4/P_2O_7) groups present in samples treated between 300 and 700 °C. Therefore, the ^{31}P peaks resonating at about −33 and −44 ppm are assigned to non-protonated environments (denoted by asterisks in Figure 14). In addition, the 2D $^{31}P-^{31}P$ spin-exchange NMR spectrum (Figure 15) of the sample treated at 700 °C, shows the coexistence of at least two distinct phases: one including resonances at about −29, −30, and −33 ppm, and the other having only one signal resonating at about −44 ppm. Finally, at 900 °C, the presence of multiple ^{31}P environments (Figure 14d) is typical of a cubic $3 \times 3 \times 3$ superstructure TiP_2O_7.[40]

Although the exothermic peak ($T \sim 880$ °C) observed in the DTA curve (Figure 7) has been largely attributed to a TiP_2O_7 phase transition,[15,17] to our knowledge, at room temperature, a unique TiP_2O_7 phase has been, at present, reported. However, the structural history of this material is very long. In 1935, from powder studies, a small cubic unit cell in space group $Pa\bar{3}$ and with $a = 7.80(1)$ Å was found for TiP_2O_7.[41] Later, in the family of tetravalent metal pyrophosphates, evidence of a possible $3 \times 3 \times 3$ superstructure at

(40) Sanz, J.; Iglesias, J. E.; Soria, J.; Losilla, E. R.; Aranda, M. A. G.; Bruque, S. *Chem. Mater.* **1997**, *9*, 996.
(41) Levi, G. R.; Peyronel, G. *Z. Kristallogr.* **1935**, *92*, 190.

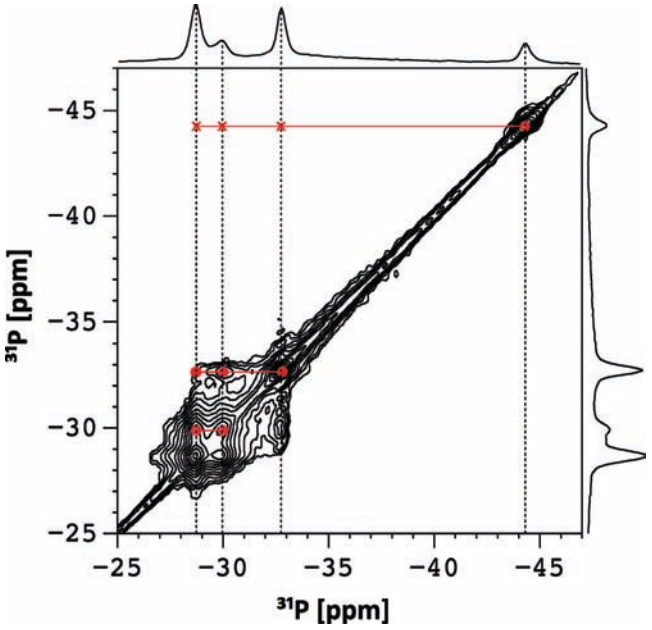

Figure 15. 2D $^{31}P-^{31}P$- spin-exchange spectrum of γ-TiP recorded at room temperature after thermal treatment at 700 °C employing a mixing time of 2 s. Filled circles represent cross-peaks between ^{31}P sites within the same phase, while crosses represent the absence of correlation between different ^{31}P sites.

room temperature was first proposed in 1963, after careful examination of powder diffraction data for GeP_2O_7.[42] Much later, X-ray powder studies combined with NMR data of TiP_2O_7,[40] and further NMR studies,[43] show a distorted structure that is less correlated to the smaller substructure. Finally, synchrotron radiation single-crystal data were reported,[44] showing the existence of at least eleven crystallographically distinct P sites. In this compound-type, a phase transition occurs at high temperatures from the superstructure to the small cubic structure (for example, at 290 °C in ZrP_2O_7).[45] However, in samples treated at 500−700 °C, our room-temperature ^{31}P NMR data (Figure 14) shows only a single resonance (at ca. −44 ppm) assignable to a novel TiP_2O_7 phase (the position corresponds well to the mean position found for 3 × 3 × 3 superstructure TiP_2O_7). For analogy with zirconium compounds, this phase may, probably, be β-TiP_2O_7 (orthorhombic β-ZrP_2O_7, where all the phosphorus are equivalent, as obtained by τ-$Zr(HPO_4)_2$ thermal treatment).[46] Now considering the $Ti(PO_4)(H_2P_2O_7)_{0.5}$ phase, the 2D $^{31}P-^{31}P$ spin-exchange NMR spectrum of γ-TiP after thermal treatment at 700 °C (Figure 15) proves that at least two distinct phases coexist. This may be supported by the following: (i) all the ^{31}P resonances above −40 ppm are correlated between each other thus constituting one phase (assigned to the $Ti(PO_4)(H_2P_2O_7)_{0.5}$), and (ii) the ^{31}P resonance at about −44 ppm, which is clearly uncorrelated to the remaining resonances, is tentatively assigned, as stated previously, to the orthorhombic β-TiP_2O_7. In our laboratories, we are now working to obtain the synthesis and structural characterization of this new titanium pyrophosphate polymorph.

Conclusion

The thermal decomposition of layered γ-titanium phosphate and, likely, that of other chemical and/or structurally related compounds, is a complex process that can only be rationalized by the tandem use of complementary experimental techniques and simulation procedures. In this work, 1D and 2D ^{31}P NMR data recorded in situ at different temperatures and after thermal treatment (up to 900 °C) aided in the γ-TiP structural description and allowed to follow quantitatively the hydration level of this material at different temperatures. A correlation between the dependence of the activation energy on the extent of conversion in the γ-TiP thermal decomposition and NMR data was reached and proved the presence of a complex multistep decomposition process, where the crystal structures of two intermediates, γ'-$Ti(PO_4)(H_2PO_4)\cdot(2-x)H_2O$ ($x \sim 1$) and $Ti(PO_4)(H_2P_2O_7)_{0.5}$, were proposed for the first time by means of structural modeling.

Acknowledgment. We thank financial support from FEDER, PTDC (Portugal), the Portuguese Foundation for Science and Technology [(FCT), ref: PTDC/QUI-QUI/100998/2008], POCI2010, FSE, Spanish *Ministerio de Educación y Ciencia* (ACI20073448000507, MAT2006-01997 and *Factoría de Crystalización − Consolider Ingenio 2010*), and *Gobierno del Principado de Asturias* (PCTI 2006-2009). We thank C. Coelho for her contribution on some NMR measurements. The authors also thank SpLine beamline staff for support during the powder XRD experiments and the financial support from MEC and the CSIC (Intramural 2004 5 OE 292) for the realization of the powder synchrotron XRD experiments.

Supporting Information Available: X-ray crystallographic data in CIF format for $Ti(PO_4)(H_2PO_4)\cdot 2H_2O$, $Ti(PO_4)(H_2PO_4)\cdot H_2O$, and $Ti(PO_4)(H_2P_2O_7)_{0.5}$. This material is available free of charge via the Internet at http://pubs.acs.org.

(42) Vollenke, H.; Wittman, A.; Nowotny, H. *Monatsh. Chem.* **1963**, *94*, 956.
(43) Helluy, X.; Marichal, A. *J. Phys. Chem. B* **2000**, *104*, 2836.
(44) Norberg, S. T.; Svensson, G.; Albertsson, J. *Acta Crystallogr., Sect. C* **2001**, *57*, 225.
(45) Korthuis, V.; Khosrovani, N.; Sleight, A. W.; Roberts, N.; Dupree, R.; Warren, W. W. *Chem. Mater.* **1995**, *7*, 412.
(46) Andersen, A. M. K.; Norby, P. *Acta Crystallogr., Sect. B* **2000**, *56*, 618.